# The Intrinsic Flexibility of the Kv Voltage Sensor and Its Implications for Channel Gating

Zara A. Sands, Alessandro Grottesi, and Mark S. P. Sansom
Department of Biochemistry, University of Oxford, Oxford OX1 3QU, United Kingdom

ABSTRACT Analysis of the crystal structures of the intact voltage-sensitive potassium channel KvAP (from *Aeropyrum pernix*) and Kv1.2 (from rat brain), along with the isolated voltage sensor (VS) domain from KvAP, raises the question of the exact nature of the voltage-sensing conformational change that triggers activation of Kv and related voltage-gated channels. Molecular dynamics simulations of the isolated VS of KvAP in a detergent micelle environment at two different temperatures (300 K and 368 K) have been used to probe the intrinsic flexibility of this domain on a tens-of-nanoseconds timescale. The VS contains a positively charged (S4) helix which is packed against a more hydrophobic S3 helix. The simulations at elevated temperature reveal an intrinsic flexibility/conformational instability of the S3a region (i.e., the C-terminus of the S3 helix). It is also evident that the S4 helix undergoes hinge bending and swiveling about its central $I^{130}$ residue. The conformational instability of the S3a region facilitates the motion of the N-terminal segment of S4 (i.e., S4a). These simulations thus support a gating model in which, in response to depolarization, an S3b-S4a "paddle" may move relative to the rest of the VS domain. The flexible S3a region may in turn act to help restore the paddle to its initial conformation upon repolarization.

## INTRODUCTION

Voltage-gated potassium (Kv) channels are integral membrane proteins that enable the passage of $K^+$ ions across cell membranes. They undergo a conformational transition (gating) which is driven by changes in the transmembrane (TM) voltage. They play a key role in the physiology of all excitable cells, for example in the nervous system and the heart. Kv channels have two principal functions: ion conduction and voltage sensing. These two functions reside in distinct but functionally coupled domains. Kv channels are made up of four identical (or similar) subunits. Each subunit is believed to contain six TM helices, called S1–S6. The S5 and S6 helices, with an intervening P-loop, form the central pore (1). The voltage sensor (VS) domain is made of helices S1–S4, with the positively charged S4 helix (which has every third residue positively charged in its N-terminal half) moving in response to a change in TM voltage to initiate the conformational change underlying gating.

Crystallographic studies of the bacterial Kv homolog, KvAP (2), have revealed that the pore domain of KvAP has an architecture similar to that of other $K^+$ channels, such as the bacterial $K^+$ channel KcsA (3). However, the exact conformation and orientation of the S1–S4 domain (i.e., the VS domain) is less certain. In particular, the structure of the VS domain within the crystal structure of the full length channel construct is somewhat at odds with aspects of available physiological and biophysical data (4). Furthermore, the conformations of the VS domain in the x-ray and single particle electron microscopy structures (5) seem to be somewhat different, implying a conformational transition associated with channel gating.

In addition to the crystal structure of the full length KvAP channel, the structure of the isolated VS has also been solved (2) (Fig. 1 *A*). Both the full length channel and the isolated VS domain structures were solved using monoclonal antibody Fab fragments to aid protein crystallization. The isolated VS domain structure is broadly consistent with a range of biophysical and physiological data and thus may represent the conformation of the VS domain under physiological conditions. Combined with the relatively high resolution (1.9 Å) of the VS structure, this makes this domain an attractive candidate for simulation studies of its conformational dynamics in the context of possible channel gating mechanisms.

The recent x-ray structure of the intact mammalian voltage-gated potassium channel Kv1.2 (6) is partially resolved in the VS domain; however, it reveals the S1, S2, S3, and S4 helices. Superimposition of the VS of Kv1.2 with the isolated VS of KvAP reveals that the basic architectures of the two proteins are similar. It is therefore likely that the Kv1.2 structure captures the VS in a native conformation. It is also evident from the Kv1.2 structure that each VS is loosely positioned against the pore-forming helices of an adjacent subunit via the S4–S5 linker. In such an arrangement the VS will be exposed to a lipid environment. In addition to this work several studies have focused on the very nature of the VS/pore domain interaction and on determining the changes in conformation and/or orientation of the VS in response to membrane depolarization (4). For example, site-directed spin labeling data (7) have been used to determine how the VS and pore domains of KvAP may pack together within a lipid bilayer environment. A number of models of the conformational change underlying Kv channel gating have been proposed on the basis of structural and other data,

*Submitted August 5, 2005, and accepted for publication November 9, 2005.*
Address reprint requests to Mark S. P. Sansom, Tel.: 44-1865-2752371; Fax: 44-1865-275273; E-mail: mark@biop.ox.ac.uk.

0006-3495/06/03/1598/09 $2.00
doi: 10.1529/biophysj.105.072199

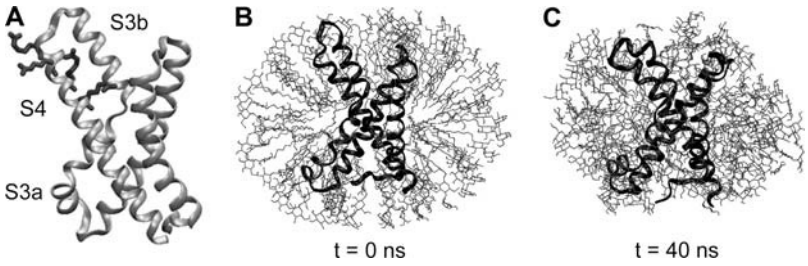


FIGURE 1 The KvAP VS. (*A*) The crystal structure (PDB code 1ORS) of the VS shown in ribbons format. The side chains of the four arginine residues in the N-terminal half of the S4 helix ($R^{117}$, $R^{120}$, $R^{123}$, $R^{126}$) are shown. (*B* and *C*) The VS embedded in a detergent (DM) micelle shown at the start ($t = 0$ ns) and end ($t = 40$ ns) of simulation VS300.

including studies of VS-directed toxins and their interactions with Kv channels (8). The models that account for the conformational changes that accompany the VS upon membrane depolarization include the S4 helical screw (9), transporter (10), paddle (11), and twisted S4 (7) models. Two of the models, namely the canonical and the transporter, sequester the gating charges from a lipid environment by packing the S4 helices tightly against S1–S3 helices and the pore lining helices. This is contrary to the Kv1.2 crystal structure finding, which reveals that the first two arginines are located on a lipid-facing surface. In the paddle and twisted S4 models the positively charged S4 helices are significantly exposed to the surrounding lipid environment, in agreement with the Kv1.2 structure. Thus, it is of some interest to determine the nature of the intrinsic flexibility of the VS domain uncoupled from the pore (gating) domain.

In this study, we use molecular dynamics (MD) simulations to explore the conformational dynamics of the VS domain. To enhance sampling of the intrinsic flexibility of the VS domain, we have performed simulations on the isolated VS domain in a detergent micelle environment. The simulations reveal that a modified ''paddle'', consisting of the C-terminal half of the S3 helix and the N-terminal half of the S4 helix, is intrinsically flexible on a nanosecond timescale. Although the gating process per se occurs on too slow a timescale (of the order of microseconds) to be addressed directly by MD simulations (which probe flexibility on a tens of ns timescale), the simulations provide valuable clues as to the nature of the voltage-gating mechanism. Furthermore, simulations offer the possibility of examining the dynamics of the VS in the in vitro environment used for purification and crystallization, namely in detergent micelles.

## METHODS

### Protein model

The initial voltage-sensing domain model (residue 19–147) was taken from the 1.9 Å isolated VS crystal structure Protein Data Bank ((PDB) code 1ORS). Side-chain ionization states were determined based on $pK_A$ calculations performed using the program WHATIF (12) combined with locally written code. All of the ionizable residues were in their default states (i.e., their ionization states were those expected at pH 7 based on the standard $pK_A$ values of the residues), except for $D^{146}$, which was judged to have approximately equal probabilities of adopting either an ionized or neutral state (see below for details).

### Setup of micelle systems

Each protein/detergent micelle was constructed using 94 DM (decyl maltoside) detergent molecules. The DM molecules were randomly rotated about their tail axes and arranged into semicircular planes, forming an expanded micelle-like torus around the isolated VS. Each detergent headgroup was approximately equidistant from its nearest neighbor. The terminal methyl groups of the DM tails were placed so that a minimum distance of 5 Å was maintained between each detergent molecule and the exterior of the isolated VS, so as to avoid unfavorable van der Waals overlaps. Similar initial protein/detergent micelle constructs have been generated in a number of other simulation studies (13,14) and have been shown to yield equilibrium structures similar to those generated by more extensive self-assembly simulations (15).

Each protein-micelle system was energy minimized and then solvated by superimposition of a box of preequilibrated SPC (16,17) water molecules, followed by removal of any water molecules too close to either protein or detergent molecules. The resultant systems were then subjected to further energy minimization. Potassium and chloride ions were added to each system by random replacement of water molecules, until a final concentration of ~0.1 M was achieved. The resultant systems were subjected to a further stage of energy minimization. This was followed by 1 ns of restrained MD during which all of the heavy (i.e., not H) protein atoms were positionally restrained. Restrained MD runs were performed at 300 K and 368 K for each protein-micelle system (Table 1). Finally, all positional restraints were removed and production run simulations were performed for each system.

### Simulation details

Simulations were performed using GROMACS 3.1 (18) (www.gromacs.org). The GROMOS96 force field (19) was used for all simulations. The parameters for DM were based on GROMOS96, supplemented with additional bond, angle, and dihedral terms to rigidify the sugar groups. Initial DM coordinates were derived from the structure of maltose when bound to a maltodextrin transport/chemosensory receptor (20) (PDB code 1ANF) combined with results from semiempirical calculations performed on the lipid chain using the CFF module in Insight II (www.accelrys.com/insight). All energy minimization procedures used <1000 steeps of steepest descent method to relax any steric conflicts generated during system setup. During restrained MD runs, harmonic restraints with force constants of 10 kJ $mol^{-1}$ $Å^{-2}$ were applied to all heavy atoms. Long-range electrostatic interactions

**TABLE 1 Summary of simulations**

| Simulation | $D^{146}$ | $T$ (K) | Duration (ns) | Cα RMSD* (all residues; Å) | Cα RMSD* (helical residues; Å) |
|---|---|---|---|---|---|
| VS300 | Ionized | 300 | 40 | 2.6 | 2.1 |
| VSH300 | Protonated | 300 | 30 | 2.7 | 2.2 |
| VS368 | Ionized | 368 | 40 | 4.2 | 3.3 |
| VSH368 | Protonated | 368 | 30 | 4.1 | 3.4 |

*Relative to the initial conformation and averaged over the final 5 ns of the simulation.

were calculated using the particle mesh Ewald method (21), with a 10 Å cutoff for the real space calculation. A cutoff of 10 Å was used for the van der Waals interactions. The simulations were performed at constant temperature, pressure, and number of particles. The temperature of the protein, detergent, and solvent (waters and ions) were separately coupled using the Nose-Hoover thermostat (22,23) at 300 K or 368 K, with a coupling constant $\tau_T = 0.1$ ps. System pressures were isotropically coupled using the Parrinello-Rahman barostat (24,25) at 1 bar with a coupling constant $\tau_P = 1$ ps and compressibility $= 4.5 \times 10^{-5}$ bar$^{-1}$. For all simulations the time step for integration was 2 fs, and the coordinates and velocities were saved every 5 ps. The LINCS algorithm (26) was used throughout to constrain bond lengths.

Simulations were performed on a 68 node PC cluster with dual Xeon4 processors. All analyses used GROMACS and/or locally written code. Simulations were analyzed by means of principal component analysis (27): trajectories were projected along selected eigenvectors to filter the relevant motions (28). The program SWINK has been used to measure the swivel and kink angles of the helices (29). Secondary structural alignments were performed using the secondary structure matching (SSM) server (30). Molecular graphics images were generated using VMD (31) or Pymol (www.pymol.org).

## RESULTS

### Simulations in detergent micelles

The pore-forming and voltage-sensing domains of Kv channels seem to be, to some extent, independent functional modules. Thus, all $K^+$ channels appear to share the same pore domain (4), whereas only Kv channels contain the VS domain. From a structural viewpoint, the isolated VS domain of KvAP forms high resolution crystals (2) and also forms a stable folded domain when in detergent micelles (2,11) and when in lipid bilayers (32). Thus, simulations of the isolated VS may provide insights into the intrinsic conformational flexibility of this domain, which in turn will inform attempts to formulate atomic resolution models of the mechanism of voltage gating of Kv channels. Furthermore, the crystal structure of the isolated VS seems to be broadly consistent with molecular physiology and spectroscopic data and thus is likely to represent a major physiological conformation of the VS when within Kv channels (33,34).

Detergents mimic a biological membrane environment and as such play an important role in a number of biochemical techniques that have been applied to the study of membrane proteins. As DM was used to solubilize both the full length KvAP molecule and its isolated VS for crystallization, we have simulated the KvAP VS in a DM micelle. The exact size of the VS-detergent micellar aggregate is unknown. Using the surface of the VS as a guide, 94 detergent molecules were needed to form a complete toroidal micelle around the protein. Relative to pure detergent micelles, increases in numbers of detergents of 10–25 have been seen for peptide-containing micelles (35). The experimentally determined size of pure DM micelles is ~70 molecules (www.anatrace.com). Thus, 94 DM molecules in a VS/DM micelle would seem to be a reasonable estimate. The geometry of protein/detergent micelles are not known in detail. Simulation studies, both of preformed (13,14) and of self-assembled (15) protein/detergent micelles, suggest an approximately toroidal geometry for the detergent, wrapped around the protein. Therefore we inserted the VS into a preformed DM micelle, using the membrane protein aromatic residues as a guide to the location of micelle around the $\alpha$-helical VS domain.

Charged residues in the VS play a crucial role in voltage sensing (36,37). Therefore $pK_A$ calculations (see Methods) were performed on the isolated VS to ascertain the most probable side-chain ionization states when the VS was placed in a membrane mimetic environment. All of the ionizable residues were predicted to exist in their default charge states, with the exception of an aspartic acid residue ($D^{146}$) which was predicted to have an approximately equal likelihood for both its ionized and protonated states (its predicted $pK_A$ was 7.9 and 5.2 in vacuo and in a membrane mimetic, respectively). We therefore have performed simulations with residue $D^{146}$ in each of these states (Table 1).

KvAP is from the thermophilic bacteria *Aeropyrum pernix*, which thrives at temperatures ~368 K (95°C) (38). Therefore, in addition to simulations at 300 K, we have run simulations at 368 K to explore the conformational dynamics of KvAP VS at a temperature closer to its physiological operating temperature and also to explore enhanced protein flexibility at the higher temperature. In total we have performed 0.14 $\mu$s of MD simulations of the KvAP VS in a detergent micelle, a system containing ~44,000 atoms.

Visual inspection of each VS/DM micelle system revealed that the initially ordered torus of detergent molecules in the micelle (Fig. 1 *B*) adjusted its shape during the course of each simulation so as to increase the solvent exposure of the ends of the helices (Fig. 1 *C*). This is comparable to the behavior observed in a number of other membrane protein/micelle simulations, e.g., of the $\beta$-barrel outer membrane protein OmpA (13) and of the $\alpha$-helical membrane protein GlpF (14), both in micelles with octyl glucoside. The shape of the detergent component of the micelles was quantified by calculation of the eccentricity, defined as $\eta = 1 - I\,I_{MIN}/I_{AVG}$ where $I_{MIN}$ is the smallest of the three principal moments of inertia ($I_1$, $I_2$, $I_3$), and $I_{AVG}$ is the average of all three. For a perfectly spherical object, $\eta = 0$. For the four simulations the initial eccentricity was $\eta \approx 0.07$. At the end of the simulations, the eccentricity was $\eta \approx 0.19$. Thus, the micelles become more ellipsoidal with time, as has also been observed with OmpA/DPC micelles (for which $\eta \approx 0.2$—see Bond and Sansom (13)) and with GlpF/OG micelles (14).

### Conformational drift

To evaluate the conformational stability of the isolated VS in these micelle simulations, we have measured the degree of drift from the initial (crystal) structure. This may be evaluated as the root mean-square deviation (RMSD) of the C$\alpha$

atoms from their coordinates at the start of the simulation (Fig. 2). The general pattern is the same in all simulations—an initial jump followed by a slower rise to a plateau. This has been observed in many MD simulations of membrane proteins, both in lipid bilayers and detergent micelles. At 300 K the C$\alpha$ RMSD over the final 5 ns (for all residues, i.e., including the loops between helices) is ~2 Å regardless of the ionization state of $D^{146}$. This is comparable to that seen for other membrane proteins in micelles (e.g., ~2 Å for GlpF (14) and a similar value for OmpA is obtained if one excludes the long flexible extracellular loops from the RMSD calculation for the latter protein (13)). Thus, even though the current simulations of the KvAP VS are 3–4 times longer than those of GlpF and OmpA, the conformational drift of the VS is about the same. We may therefore conclude that the VS is conformationally stable in DM micelles on a ~40 ns timescale at 300 K.

At the higher temperature, the RMSDs for both simulations are substantially higher (~4 Å). (This is comparable to the figure for OmpA at 300 K if the flexible loops are included in the calculation.) However, if only the $\alpha$-helical regions are taken into consideration, the final C$\alpha$ RMSDs are ~3 Å. This indicates that at 368 K the greater structural drift is largely, but not entirely, due to conformational changes occurring in the loop regions. Again, the protonation state of $D^{146}$ does not seem to influence the conformational drift at the higher temperature.

In summary, from consideration of conformational drift we can see that removal of the VS from its crystallographic interactions with the Fab molecule and embedding it in a detergent micelle does not lead, on a ~40 ns timescale, to a substantial change in conformation even at an elevated temperature. By way of comparison, chymotrypsin inhibitor 2 has been observed to unfold on a ~25 ns timescale in simulations at 373 K (39). Taken together, this suggests that the isolated VS domain is intrinsically stable in a micelle environment.

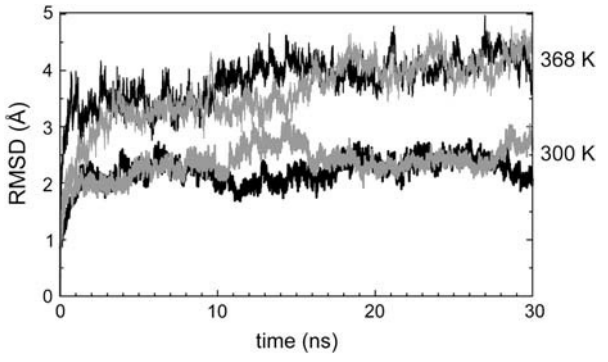


FIGURE 2 Conformational drift during the simulations, measured as C$\alpha$ RMSD from the initial structure. The C$\alpha$ RMSDs over 30 ns are shown for simulations VS300 (*solid, lower curve*), VSH300 (*shaded, lower curve*), VS368 (*solid, upper curve*), and VSH368 (*shaded, upper curve*).

## Secondary structure and flexibility

A more detailed analysis of the simulations reveals the relative flexibility of the different regions of the VS. Analysis of the secondary structural elements as defined by DSSP (40) (Fig. 3 *A*) showed that helices S1, S2, and S4 were stable over the course of each simulation, regardless of the temperature or protonation state of $D^{146}$. In contrast, the S3 helix (which in the crystal structure is distorted to form distinct S3a and S3b helices, Fig. 3 *D*) and the S3/S4 loop show enhanced flexibility at the higher temperature. In particular, S3a unfolds at 368 K, regardless of the protonation state of

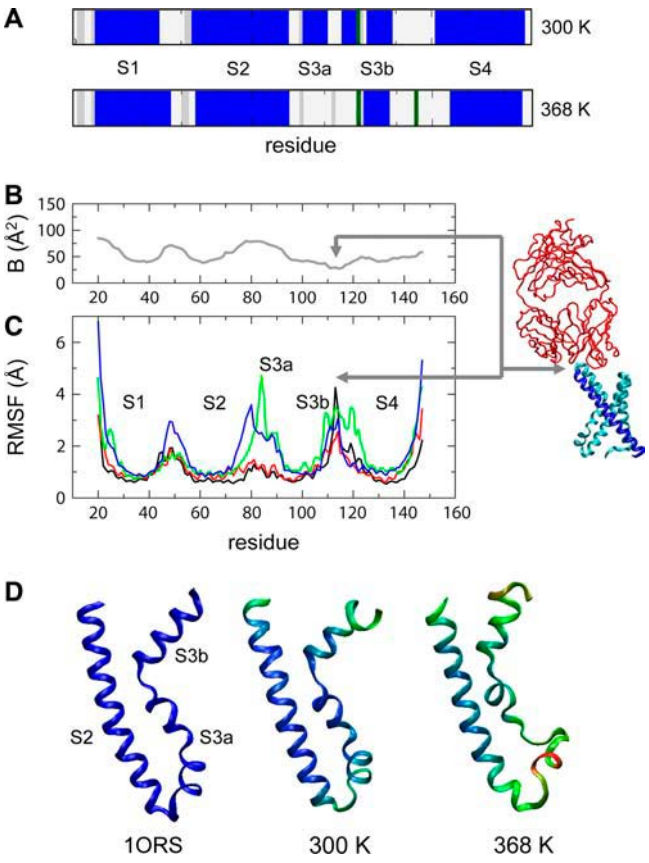


FIGURE 3 Secondary structure and conformational flexibility during the simulations. (*A*) Time averaged secondary structure for simulations VS300 and VS368. Secondary structure elements persisting for ≥90% of the simulation time are shown as blue, $\alpha$-helix; gray, $3_{10}$ helix; green, bend; and white, coil. (*B*) Crystallographic temperature factor *B* of C$\alpha$ atoms as a function of residue number, and (*C*) conformational flexibility measured as RMSF of the C$\alpha$ atoms versus their average position as a function of residue number (color code: *black*, VS300; *red*, VSH300; *green*, VS368; *blue*, VSH368). The structural diagram to the right shows the VS (*blue*) and the bound Fab molecule (*red*). The main interaction of the latter with the VS is via contacts at the loop between S3b and S4, as indicated by the gray arrows. (*D*) Changes in the secondary structure of the S3 region of the VS. The crystal structure (1ORS) and the final structures from simulations VS300 and VS368 are compared for S2 and for S3. The residues for the two simulations are colored according to the magnitude of RMSFs experienced by the C$\alpha$s during the course of each simulation (on a scale from *blue* = 0.0 Å to *red* = 4.8 Å). The loss of helicity in S3a of VS368 is evident.

$D^{146}$. (There is also some loss of helicity from the N-terminus of S4 at 368 K, but only if $D^{146}$ is ionized.) Thus, the elevated temperature simulations suggest a degree of conformational instability for S3a. Interestingly, a consensus TM helix secondary structure prediction analysis of KvAP (41) suggested that S3a may not form a canonical TM helix.

It is possible to explore in more detail the relative flexibility of different regions of the VS by calculation of the root mean-square fluctuation (RMSF) of each C$\alpha$ atom from its time averaged coordinate (Fig. 3 *C*). The overall pattern for each simulation is as anticipated, with higher RMSFs for the loops and lower RMSFs for the cores of the $\alpha$-helices. However, there are some more significant details. First, the S2/S3a loop and the S3a region show a significantly higher RMSF at 368 K than at 300 K. This is consistent with the secondary structure analysis and suggests that S3a is unstable at the higher temperature. The second significant detail is that the S3b-S4 loop shows a relatively high RMSF in each of the simulations.

A comparison with the corresponding crystallographic temperature factor (B-value; Fig. 3 *B*) profile is informative. Of course, one should guard against overinterpretation of comparisons of crystallographic B-values and simulation RMSFs. However, a striking difference in the overall profiles is evident, namely that the crystallographic B-value for the S3b/S4 loop is low relative to the remainder of the protein, whereas the RMSF for this region is high relative to the protein as a whole. As shown in the inset in Fig. 3, the S3b-S4 loop corresponds to the primary interaction between the VS and the Fab molecule. Thus it would seem that either the intrinsic flexibility of the S3b/S4 loop is suppressed within the Fab/VS crystal and/or the local conformation of this region in the crystal may be altered relative to its equilibrium structure in the micellar environment. It is of possible functional significance that this region, the S3b-S4 loop, corresponds to the tip of the voltage-sensing paddle that is suggested to be capable of changing its conformation/orientation relative to the membrane in the paddle model of voltage gating (11).

The results of the analysis of secondary structure and flexibility may be summarized with reference to Fig. 3 *D*. Comparison of the crystallographic structure with those at the end of the VS300 and VS368 simulations for the S2–S3 region shows that there is a local change in conformation in S3a and a local distortion of the C-terminus of S3b. Thus, the simulations reveal that the S3a and S3b helices possess a degree of conformational flexibility. As we will see, this is important in allowing the S4 helix to move relative to the remainder of the VS domain, a process that is in turn of relevance to voltage gating in the channel.

The crystal structure of the isolated VS domain of KvAP superimposed on the corresponding VS domain of Kv1.2 reveals that the two structures are similar (RMSD 2.9 Å). However, they diverge most notably in the region of the S3 helix (Fig. 4). Thus, the Kv1.2 crystal structure has captured the S3 helix in a different conformation from that of KvAP, which may further support the notion of a flexible S3 helix.

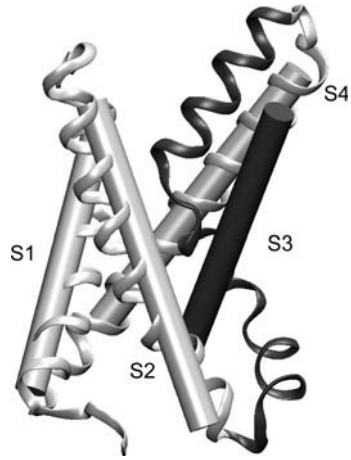


FIGURE 4 Comparison of the VS domain structures of KvAP (*ribbons*) and Kv1.2 (*cylinders*). The S3 helix is shown in dark gray, the remainder of the structure in pale gray. The two structures were superimposed using SSM (30).

## S4 helix movements and flexibility

The S4 helix is believed to move relative to the remainder of the channel in some way that couples voltage-sensing to channel gating. It is therefore useful to examine the simulations from the perspective of the intrinsic flexibility of the S4 helix, and in particular to see whether or not it behaves as a rigid helical rod.

Simple visual examination of snapshots of S4 suggests a degree of hinge bending may occur in this helix about the central $I^{130}$ residue (Fig. 5 *A*). To explore this aspect of S4 dynamics in more detail, we employed principal components analysis (PCA) to reveal the major motions of the helix. We combined PCA with analysis of the motions of S4 in terms of helix kink and swivel. Analyzing TM helix distortions in terms of kink and swivel angles has been employed to explore proline-induced distortions of TM helices in x-ray structures of membrane proteins (29) and more recently in analysis of M2 helix hinge bending as the basis of channel gating in simulations of inward rectifier $K^+$ channels (42). If we take the motions of S4 represented by the first two eigenvectors (together these account for ~50% of the motion observed in the simulations) and analyze these in terms of kink and swivel angle, we see clear evidence for both swivel motion and, to a lesser extent, kink motion about the center of S4 (Fig. 5, *B* and *C*). The central hinge point seems to be around residue $I^{130}$, i.e., in the center of the S4 helix. Thus, the S4 helix does not behave as a rigid rod but rather as two semirigid $\alpha$-helical segments connected by a central molecular hinge. We note that the flexibility observed in the S3b/S4 loop may facilitate such motions of S4.

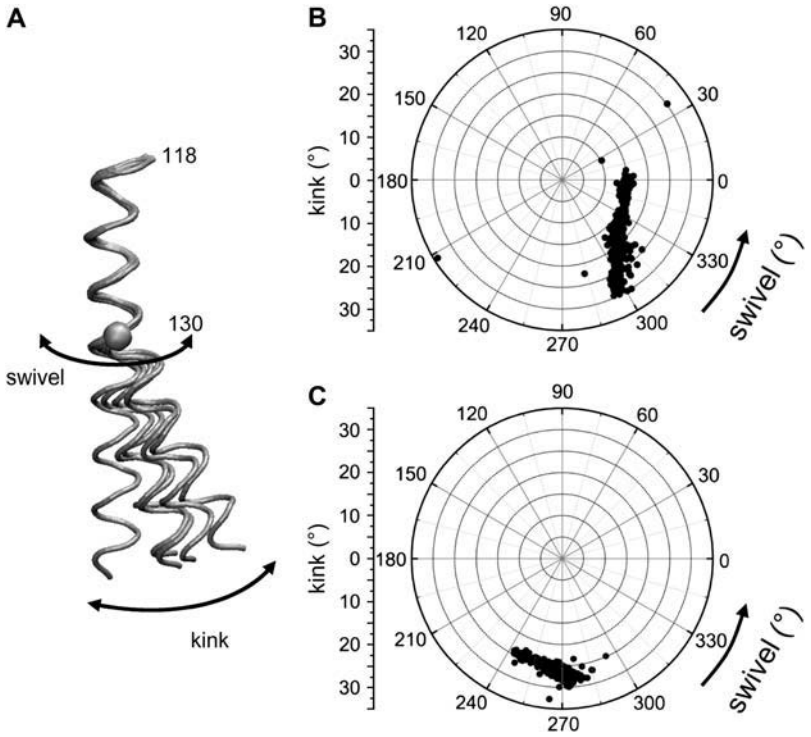


FIGURE 5 Swivel and kink analysis of helix S4. (*A*) Snapshots of S4 from simulation VS300 (not post-PCA), saved every 8 ns from 2 ns onwards (i.e., 2, 10, 18, 26, and 34 ns). The helices are fitted on the N-terminal segment of S4 (118–130) to illustrate the hinge-bending motion about $I^{130}$ (indicated by the sphere). The definition of the molecular hinge in the center of helix S4 is shown, indicating how the motions may be decomposed into swivel and kink angles. (*B* and *C*) Examples of motions of S4 in the simulations revealed by PCA, showing a predominant kink (*B*, eigenvector 1 of simulation VS368) and a predominant swivel (*C*, eigenvector 1 of simulation VSH368). Each point represents the kink and swivel angles, plotted as polar coordinates, of a snapshot structure saved every 50 ps from the PCA-filtered trajectory.

## Water penetration

There have been a number of suggestions that the S4 helix sits within a water-filled crevice, which therefore focuses the TM voltage difference on a narrow central region of the S4 helix (4,10). This is evidently of some importance for possible voltage sensing/gating models of Kv and related channels (43). We have used water penetration within the protein/detergent micelles as a measure of the degree of crevice formation in the VS. As can be seen (Fig. 6 *A*), a number of water molecules do infiltrate the VS, forming hydrogen bonds with, e.g., $R^{117}$, $R^{120}$, $R^{123}$, and $R^{126}$ of the N-terminal half of S4 (Table 2). Thus, our simulations indicate that hydrogen-bonding interactions with such waters may help to stabilize the positively charged S4 helix within a bilayer-like environment. Preliminary analysis of simulations of the VS in a lipid bilayer support this claim (Z. A. Sands and M. S. P. Sansom, unpublished results). Of course, in the intact channel the VS is packed next to the core pore-forming domain of the protein. However, it is likely that the micelle mimics the environment provided by the remainder of the protein in the intact channel.

Analysis of the radius profile along the length of the presumed crevice (Fig. 6 *B*) reveals that there is a central constriction which, averaged across the simulation, is significantly narrower than the radius of a water molecule (~1.4 Å). Thus the voltage drop across the membrane must occur over a region at least ~12 Å thick around S4. The central region corresponds to a salt bridge between a side chain in S2 ($D^{62}$) and a side chain in S4 ($R^{133}$; see Fig. 6 *C*), which is maintained throughout the course of each simulation. This

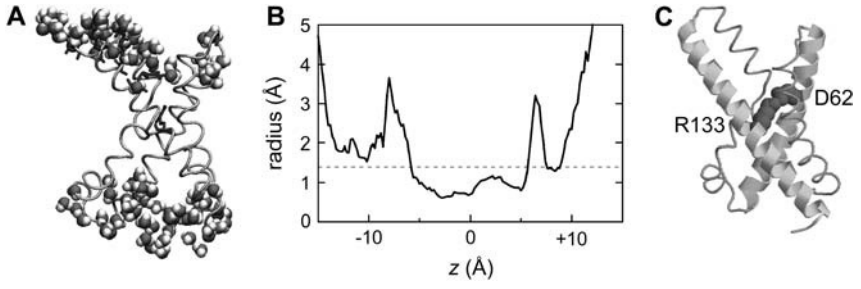


FIGURE 6 Pore-like region formed within the VS. (*A*) Snapshot from simulation VS300 at 40 ns showing water molecules within 1 Å of the protein and within 2 Å of the arginines side chains. Two clusters of water molecules may be seen on either side of the central constriction. (*B*) Radius profile of the pore-like region through the center of VS. The radius (the VS300 simulation average) is shown as a function of position along the *z* axis, which runs parallel to the axis of the pore. The broken line indicates the radius of a water molecule. (*C*) Diagram of the VS crystal structure showing the central salt bridge formed by the side chains of $D^{62}$ (from S2) and $R^{133}$ (from S4). Helices S2 and S4 are shown as ribbons. This salt bridge constricts the pore in its center. The salt bridge is present throughout the VS300 and VSH300 simulations and is present through most of the 368 K simulations, with occasional disruptions of duration ~1–2 ns.

**TABLE 2 H-bonding to S4 arginine side chains**

| | Mean number of H-bonds | |
|---|---|---|
| Arginine | water | DM |
| 117 | 4.3 | 1.4 |
| 120 | 4.3 | 0.6 |
| 123 | 3.4 | 0.5 |
| 126 | 2.8 | 0.1 |

The table shows the mean number of H-bonds formed between the gating charge arginine side chains and waters or detergent (DM) molecules for simulation VS300.

salt bridge holds S2 and S4 in close proximity and prevents water from passing from one side to the other of the crevice. It is noteworthy that the central hinge in S4 (at residue $I^{130}$) is just one turn of the helix before $R^{133}$. Thus the two halves of S4 are connected by a hinge that fits within the narrow central region of the water penetrable crevice.

## Detergent interactions

It is of some interest whether the gating charges on S4 are able to favorably interact with the micelle environment or whether they remain buried within the interior of the VS. In the paddle and the twisted S4 models, the charged S4 helices are significantly exposed to the surrounding lipid environment during their translocation from one side of the membrane to the other. Therefore favorable interactions between the gating charges and the lipid environment could significantly lower the energy barrier to channel activation. Analysis of the hydrogen-bonding patterns reveals that the side chains of Arg's 117, 120, 123, and 126 are able to form multiple hydrogen bonds with the uncharged headgroups of the decyl maltoside detergent molecules (Table 2).

## DISCUSSION

This set of simulations reveals the intrinsic dynamics of the KvAP VS domain. By focusing our simulations on the VS, rather than the intact channel (44), we have taken advantage of the higher resolution of the VS domain structure, which allows for more accurate simulations. By embedding the VS within a detergent micelle, the membrane-mimetic environment is able to more fully relax around the protein on the timescale accessible to current simulations, thus facilitating possible conformational transitions in the VS. Also, by using a suitable detergent our simulations stay close to experimental (in vitro) reality. The use of high temperature simulations (possible because of the thermophilic nature of *A. pernix*) helped us to more fully explore the conformational flexibility of the VS.

It is important to consider the likely effects of a detergent micelle environment on the conformational dynamics of the VS domain. Detergent micelles are widely employed in biochemical studies of membrane proteins (45), for example in NMR studies of membrane proteins (46). Whilst a detergent micelle provides a mimic of the lipid bilayer environment, both NMR (47) and simulation (13) studies suggest a small increase in protein flexibility in the micelle relative to the bilayer. It is this which we have attempted to exploit to explore the intrinsic flexibility of the VS. Of course, in the intact Kv channel this flexibility will be coupled to conformational changes leading to channel gating. This is likely to occur on a significantly longer timescale ($\sim$1 $\mu$s or more).

There are two key results which emerge from our simulations of the isolated VS. The first is the intrinsic flexibility/conformational instability of the S3a region. The second is the hinge bending and swiveling motion of the S4 helix about the central $I^{130}$ residue (see Fig. 7). The latter result correlates well with recent results from site-directed spin labeling experiments (7), which have been interpreted in terms of a swivel-like distortion in the center of S4. The overall model that emerges is of a VS domain which exhibits a limited degree of flexibility. The S4 helix is able to kink/swivel about a central ($I^{130}$) hinge and sits at the center of a crevice that can be penetrated by water at either end. The conformational instability of the S3a region facilitates the motion of the N-terminal segment of S4 (i.e., S4a) linked to S3b.

It is tempting to speculate on the implications of our simulations for possible gating models of Kv channels. Although one must remember that the simulations are of the isolated VS domain in a micelle (i.e., in vitro) environment, they do reveal aspects of the intrinsic flexibility of this domain that are likely to be of relevance to the full channel protein in a lipid bilayer. Overall, our simulations thus seem to support a modified model of an S3b-S4a ''paddle'' that can move relative to the rest of the VS domain (Fig. 8). We would suggest that the positively charged S4 helix may respond to membrane depolarization by its N-terminal S4a segment swiveling relative to the S4b region, which remains

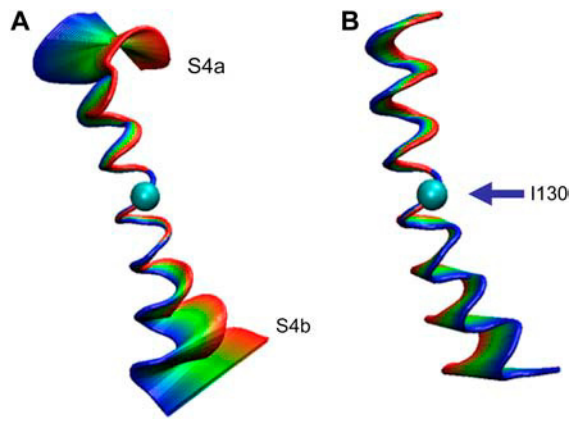


FIGURE 7 Kv channel voltage-sensing domain conformational dynamics. KvAP S4 helix hinge bending about residue $I^{130}$, as revealed by eigenvector 1 of simulation *A* VS368 and *B* VSH368. The colors indicate the range of motions represented by this eigenvector.

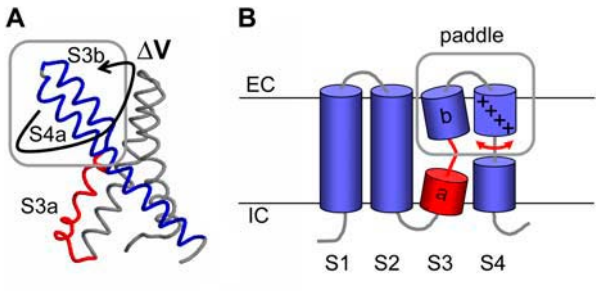


FIGURE 8 Possible gating model for Kv channels. (*A*) The VS domain paddle is formed by the S3b and S4a helices (in *blue*). The S3a segment is in red. The positively charged S4 helix is suggested to respond to membrane depolarization ($\Delta V$) by the S4a region swiveling relative to the S4b region, which remains fixed relative to the remainder of the VS. The conformational flexibility of S3a may provide a restoring spring able to return the voltage-sensing paddle (formed by S3b-S4a) to its initial conformation once the resting membrane potential is restored. (*B*) Schematic diagram of the VS TM topology, colored on conformational flexibility (*blue*, low; *red*, high), and indicating the hinge region that divides S4 into S4a and S4b.

fixed relative to the remainder of the VS. The conformational flexibility of S3a that we have observed may provide a restoring ''spring'' which facilitates the return of the voltage-sensing paddle (formed by S3b-S4a) to its initial conformation once the resting membrane potential is restored.

Studies of toxins that interact with the VS (e.g., VSTX1 (8), hanatoxin (48), and SGTX1 (49)) have been used to probe the location of the paddle relative to the membrane. It is thought that these small peptide toxins partition to the water/bilayer interface, with their hydrophobic residues pointing down toward the hydrophobic core of the bilayer ((50); D. Bemporad, Z. A. Sands, C. L. Wee, A. Grottesi, and M. S. P. Sansom, unpublished results). Mutational studies on these VS-binding toxins combined with mutational studies of Kv channels point to an interaction between polar/charged residues on the toxin surface with residues in the S3b helix of the VS (8,51,52). Together these studies suggest that the tip of the gating paddle, as defined by S3b, is located at the extracellular interfacial region of the membrane.

Furthermore, recent topological experiments suggest that despite the presence of basic side chains, an S4 helix can insert into a lipid bilayer (53). This is of particular interest given that we observe water molecules penetrating the VS/detergent micelle to solvate the charged residues on S4. This suggests that comparative simulations of S4, of the VS domain, and of the intact channel in bilayer versus micelle may reveal aspects of the stability of the S4 helix in different membrane environments. There have also been a number of simulations of KvAP and related channels, based on the crystal structure of the intact channel protein (44,54,55). Although it is difficult to evaluate the relationship of such simulations to the physiological conformations of Kv channels, they do suggest a complex interplay between VS domain, water molecules, and the membrane environment during voltage sensing.

Taken together with the current simulation studies, this body of data suggests a modified paddle model in which the intrinsic flexibility of the VS domain enables the S3b-S4a helical hairpin to move relative to the bilayer and the remainder of the channel protein in response to a change in transbilayer voltage. Such a mechanism could result in the S3b-S4a helical hairpin, changing its degree of water and bilayer exposure during the voltage-sensing transition. Further studies, both experimental and computational, are needed to unpack the exact nature of the changes in protein conformation, and in protein/water/lipid interactions, that occur during voltage sensing.

Many thanks to all of our colleagues for their helpful comments on this work, especially Peter Bond.

This work was supported by funding from The Welcome Trust.

## REFERENCES

1. Yellen, G. 2002. The voltage-gated potassium channels and their relatives. *Nature*. 419:35–42.
2. Jiang, Y., A. Lee, J. Chen, V. Ruta, M. Cadene, B. T. Chait, and R. Mackinnon. 2003. X-ray structure of a voltage-dependent $K^+$ channel. *Nature*. 423:33–41.
3. Zhou, Y., J. H. Morais-Cabral, A. Kaufman, and R. MacKinnon. 2001. Chemistry of ion coordination and hydration revealed by a $K^+$ channel-Fab complex at 2.0 Å resolution. *Nature*. 414:43–48.
4. Swartz, K. J. 2004. Towards a structural view of gating in potassium channels. *Nat. Rev. Neurosci*. 5:905–916.
5. Jiang, Q. X., D. N. Wang, and R. MacKinnon. 2004. Electron microscopic analysis of KvAP voltage-dependent $K^+$ channels in an open conformation. *Nature*. 430:806–810.
6. Long, S. B., E. B. Campbell, and R. MacKinnon. 2005. Crystal structure of a mammalian voltage-dependent *Shaker* family $K^+$ channel. *Science*. 309:897–902.
7. Cuello, L. G., D. M. Cortes, and E. Perozo. 2004. Molecular architecture of the KvAP voltage-dependent $K^+$ channel in a lipid bilayer. *Science*. 306:491–495.
8. Lee, S. Y., and R. MacKinnon. 2004. A membrane-access mechanism of ion channel inhibition by voltage sensor toxins from spider venom. *Nature*. 430:232–235.
9. Gandhi, C. C., and E. Y. Isacoff. 2002. Molecular models of voltage sensing. *J. Gen. Physiol*. 120:455–463.
10. Starace, D. M., and F. Bezanilla. 2004. A proton pore in a potassium channel voltage sensor reveals a focused electric field. *Nature*. 427: 548–553.
11. Jiang, Y., V. Ruta, J. Chen, A. G. Lee, and R. Mackinnon. 2003. The principle of gating charge movement in a voltage-dependent $K^+$ channel. *Nature*. 423:42–48.
12. Vriend, G. 1990. WhatIf—a molecular modeling and drug design program. *J. Mol. Graph*. 8:52–56.
13. Bond, P. J., and M. S. P. Sansom. 2003. Membrane protein dynamics vs. environment: simulations of OmpA in a micelle and in a bilayer. *J. Mol. Biol*. 329:1035–1053.
14. Patargias, G., P. J. Bond, S. D. Deol, and M. S. P. Sansom. 2005. Molecular dynamics simulations of GlpF in a micelle vs. in a bilayer: conformational dynamics of a membrane protein as a function of environment. *J. Phys. Chem. B*. 109:575–582.
15. Bond, P. J., J. M. Cuthbertson, S. D. Deol, and M. S. P. Sansom. 2004. MD simulations of spontaneous membrane protein/detergent micelle formation. *J. Am. Chem. Soc*. 126:15948–15949.

16. Berendsen, H. J. C., J. P. M. Postma, W. F. van Gunsteren, and J. Hermans. 1981. Intermolecular Forces. Reidel, Dordrecht, The Netherlands.

17. Berweger, C. D., W. F. van Gunsteren, and F. Mullerplathe. 1995. Force-field parametrization by weak-coupling—reengineering SPC water. *Chem. Phys. Lett.* 232:429–436.

18. Lindahl, E., B. Hess, and D. van der Spoel. 2001. GROMACS 3.0: a package for molecular simulation and trajectory analysis. *J. Mol. Model. (Online).* 7:306–317.

19. van Gunsteren, W. F., P. Kruger, S. R. Billeter, A. E. Mark, A. A. Eising, W. R. P. Scott, P. H. Huneberger, and I. G. Tironi. 1996. Biomolecular Simulation: The GROMOS96 Manual and User Guide. Biomos & Hochschulverlag AG an der ETH Zurich, Groningen and Zurich.

20. Quiocho, F. A., J. C. Spurlino, and L. E. Rodseth. 1997. Extensive features of tight oligosaccharide binding revealed in high-resolution structures of the maltodextrin transport/chemosensory receptor. *Structure.* 5:997–1015.

21. Darden, T., D. York, and L. Pedersen. 1993. Particle mesh Ewald—an N.log(N) method for Ewald sums in large systems. *J. Chem. Phys.* 98:10089–10092.

22. Nose, S. 1984. A molecular dynamics method for simulations in the canonical ensemble. *Mol. Phys.* 52:255–268.

23. Hoover, W. G. 1985. Canonical dynamics: equilibrium phase-space distributions. *Phys. Rev.* A31:1695–1697.

24. Parrinello, M., and A. Rahman. 1981. Polymorphic transitions in single-crystals—a new molecular-dynamics method. *J. Appl. Phys.* 52:7182–7190.

25. Nose, S., and M. L. Klein. 1983. Constant pressure molecular-dynamics for molecular-systems. *Mol. Phys.* 50:1055–1076.

26. Hess, B., H. Bekker, H. J. C. Berendsen, and J. G. E. M. Fraaije. 1997. LINCS: a linear constraint solver for molecular simulations. *J. Comput. Chem.* 18:1463–1472.

27. Garcia, A. E. 1992. Large-amplitude nonlinear motions in proteins. *Phys. Rev. Lett.* 68:2696–2699.

28. Amadei, A., A. B. M. Linssen, and H. J. C. Berendsen. 1993. Essential dynamics of proteins. *Proteins.* 17:412–425.

29. Cordes, F. S., J. N. Bright, and M. S. P. Sansom. 2002. Proline-induced distortions of transmembrane helices. *J. Mol. Biol.* 323:951–960.

30. Krissinel, E., and K. Henrick. 2004. Secondary structure matching (SSM), a new tool for fast protein structure alignment in three dimensions. *Acta Crystallogr. D.* 60:2256–2268.

31. Humphrey, W., A. Dalke, and K. Schulten. 1996. VMD—visual molecular dynamics. *J. Mol. Graph.* 14:33–38.

32. Cuello, L., D. M. Cortes, and E. Perozo. 2005. Structure and dynamics of the KvAP voltage sensor domain reconstituted in lipid bilayers. *Biophys. J.* 86:458A. (Abstr.)

33. Sands, Z., A. Grottesi, and M. S. P. Sansom. 2005. Voltage-gated ion channels. *Curr. Biol.* 15:R44–R47.

34. Grottesi, A., Z. Sands, and M. S. P. Sansom. 2005. Potassium channels: complete and undistorted. *Curr. Biol.* 15:R771–R774.

35. Beswick, V., R. Guerois, F. Cordier-Ochsenbein, Y. M. Coic, T. Huynh-Dinh, J. Tostain, J. P. Noel, A. Sanson, and J. M. Neumann. 1998. Dodecylphosphocholine micelles as a membrane-like environment: new results from NMR relaxation and paramagnetic relaxation enhancement analysis. *Eur. Biophys. J.* 28:48–58.

36. Seoh, S. A., D. Sigg, D. M. Papazian, and F. Bezanilla. 1996. Voltage-sensing residues in the S2 and S4 segments of the Shaker $K^+$ channel. *Neuron.* 16:1159–1167.

37. Bezanilla, F. 2000. The voltage sensor in voltage-dependent ion channels. *Physiol. Rev.* 80:555–592.

38. Sako, Y., N. Nomura, A. Uchida, Y. Ishida, Y. Morii, Y. Koga, T. Hoaki, and T. Maruyama. 1996. *Aeropyrum pernix* gen. nov., sp. nov., a novel aerobic hyperthermophilic archaeon growing at temperatures up to 100°C. *Int. J. Syst. Bacteriol.* 46:1070–1077.

39. Day, R., B. J. Bennion, S. Ham, and V. Daggett. 2002. Increasing temperature accelerates protein unfolding without changing the pathway of unfolding. *J. Mol. Biol.* 322:189–203.

40. Kabsch, W., and C. Sander. 1983. Dictionary of protein secondary structure: pattern-recognition of hydrogen-bonded and geometrical features. *Biopolymers.* 22:2577–2637.

41. Cuthbertson, J. M., D. A. Doyle, and M. S. P. Sansom. 2005. Transmembrane helix prediction: a comparative evaluation and analysis. *Protein Eng. Des. Sel.* 18:295–308.

42. Grottesi, A., C. Domene, and M. S. P. Sansom. 2005. Conformational dynamics of M2 Helices in KirBac channels: helix flexibility in relation to gating via molecular dynamics simulations. *Biochemistry.* 44: 14586–14594.

43. Nguyen, T. P., and R. Horn. 2002. Movement and crevices around a sodium channel S3 segment. *J. Gen. Physiol.* 120:419–436.

44. Monticelli, L., K. M. Robertson, J. L. MacCallum, and D. P. Tieleman. 2004. Computer simulation of the KvAP voltage-gated potassium channel: steered molecular dynamics of the voltage sensor. *FEBS Lett.* 564:325–332.

45. Garavito, R., and S. Ferguson-Miller. 2001. Detergents as tools in membrane biochemistry. *J. Biol. Chem.* 276:32403–32406.

46. Fernandez, C., C. Hilty, G. Wider, and K. Wuthrich. 2002. Lipid-protein interactions in DHPC micelles containing the integral membrane protein OmpX investigated by NMR spectroscopy. *Proc. Natl. Acad. Sci. USA.* 99:13533–13537.

47. Arora, A., F. Abildgaard, J. H. Bushweller, and L. K. Tamm. 2001. Structure of outer membrane protein A transmembrane domain by NMR spectroscopy. *Nat. Struct. Biol.* 8:334–338.

48. Takahashi, H., J. I. Kim, H. J. Min, K. Sato, K. J. Swartz, and I. Shimada. 2000. Solution structure of hanatoxin1, a gating modifier of voltage-dependent $K^+$ channels: common surface features of gating modifier toxins. *J. Mol. Biol.* 297:771–780.

49. Lee, C. W., S. Kim, S. H. Roh, H. Endoh, Y. Kodera, T. Maeda, T. Kohno, J. M. Wang, K. J. Swartz, and J. I. Kim. 2004. Solution structure and functional characterisation of SGTx1, a modifier of Kv2.1 channel gating. *Biochemistry.* 43:890–897.

50. Jung, H. J., J. Y. Lee, S. H. Kim, Y. J. Eu, S. Y. Shin, M. Milescu, K. J. Swartz, and J. I. Kim. 2005. Solution structure and lipid membrane partitioning of VSTx1, an inhibitor of the KvAP potassium channel. *Biochemistry.* 44:6015–6023.

51. Ruta, V., and R. MacKinnon. 2004. Localization of the voltage-sensor toxin receptor on KvAP. *Biochemistry.* 43:10071–10079.

52. Lee, H. C., J. M. Wang, and K. J. Swartz. 2004. Interaction between extracellular hanatoxin and the resting conformation of the voltage-sensor paddle in Kv channels. *Neuron.* 40:527–536.

53. Hessa, T., S. H. White, and G. von Heijne. 2005. Membrane insertion of a potassium-channel voltage sensor. *Science.* 307:1427.

54. Tieleman, D. P., K. M. Robertson, J. L. Maccallum, and L. Monticelli. 2004. Computer simulations of voltage-gated potassium channel KvAP. *Int. J. Quantum Chem.* 100:1071–1078.

55. Treptow, W., B. Maigret, C. Chipot, and M. Tarek. 2004. Coupled motions between pore and voltage-sensor domains: a model for Shaker B, a voltage-gated potassium channel. *Biophys. J.* 87:2365–2379.